CMS Physics Analysis Summary

Contact: cms-pag-conveners-exotica@cern.ch 2016/08/04

Search for narrow resonances decaying to dijets in pp collisions at $\sqrt{s} = 13$ TeV using 12.9 fb^{-1}

The CMS Collaboration

Abstract

A search is presented for narrow resonances decaying to dijet final states in proton-proton collisions at $\sqrt{s} = 13$ TeV from an integrated luminosity of 12.9 fb^{-1}. Results are presented for two searches. A low-mass search, for a resonance mass between 0.6 TeV and 1.6 TeV, is performed using dijets that are reconstructed from calorimeter information in the high-level trigger. A high-mass search, for resonances with mass above 1.6 TeV, is performed using dijets reconstructed with the particle flow algorithm from the normal reconstruction chain. The pseudorapidity separation of the two jets is required to satisfy $|\Delta\eta_{jj}| < 1.3$ with each jet inside the region $|\eta| < 2.5$. The spectra are well described by a smooth parameterization and no significant evidence for new particle production is observed. Upper limits at 95% confidence level are reported on the production cross section times branching ratio to dijets times acceptance of the $|\Delta\eta_{jj}|$ and $|\eta|$ cuts for narrow resonances from quark-quark, quark-gluon and gluon-gluon final states. When interpreted in the context of specific models, the limits exclude string resonances with masses below 7.4 TeV, scalar diquarks below 6.9 TeV, axigluons and colorons below 5.5 TeV, excited quarks below 5.4 TeV, color-octet scalars below 3.0TeV, W$'$ bosons below 2.7 TeV, Z$'$ bosons below 2.1 TeV and between 2.3 to 2.6 TeV, and RS gravitons below 1.9 TeV, extending previously published limits in the dijet channel.

1 Introduction

Deep inelastic proton-proton (pp) collisions often produce two or more energetic jets when the constituent partons are scattered with large transverse momenta (p_T). The invariant mass m_{jj} of the pair of jets having the largest values of p_T in the event (the dijet) has a spectrum that is predicted by quantum chromodynamics (QCD) to fall steeply and smoothly with increasing dijet mass. Many extensions of the standard model predict the existence of new massive particles that couple to quarks (q) and gluons (g) and can be detected as resonances in the dijet mass spectrum. Here we report a search for narrow resonances, those with natural widths that are small compared to the experimental resolution.

A CMS publication at $\sqrt{s} = 8\,\text{TeV}$ using the data scouting technique searched for dijet resonances with invariant mass between 0.5 TeV and 1.6 TeV [1]. Here we conduct a similar *low-mass* search for resonances with mass between 0.6 TeV and 1.6 TeV from $12.9\,\text{fb}^{-1}$ of data collected at $\sqrt{s} = 13\,\text{TeV}$ in 2016 using jets reconstructed from the calorimeter energy alone. Results are compared with a recent trigger level search at $\sqrt{s} = 13\,\text{TeV}$ by ATLAS [2].

Analyses at $\sqrt{s} = 13\,\text{TeV}$ have searched for dijet resonances with masses above 1.5 TeV at CMS [3] and above 1.2 TeV at ATLAS [4] and have extended the limits on models of dijet resonances to higher masses than the run 1 searches from CMS [5–9] and ATLAS [10–14]. Dijet resonance searches have so far used the strategies reviewed in Ref. [15]. Here we present a similar *high-mass* search for dijet resonances above 1.6 TeV using $12.9\,\text{fb}^{-1}$ of data collected at $\sqrt{s} = 13\,\text{TeV}$ in 2016 and using jets reconstructed with the particle-flow algorithm [16, 17].

We present model-independent searches and, in addition, consider the following models of s-channel dijet resonances: string resonances [18, 19], scalar diquarks [20], axigluons [21, 22], colorons [22, 23], excited quarks (q^*) [24, 25], color-octet scalars [26], new gauge bosons (W' and Z') [27], and Randall–Sundrum (RS) gravitons (G) [28]. We note that the anomalous coupling of the color-octet scalar model used is $k_s^2 = 1/2$ [29], reducing the width and cross section of this model by a factor of 1/2 compared to our previous searches, and otherwise the specific choices of parameters for the models are the same as our previous searches and can be found in Ref. [7].

2 Detector

The CMS detector and its coordinate system, including the azimuthal angle ϕ (in radians) and the pseudorapidity η, are described in detail in Ref. [30]. The central feature of the CMS apparatus is a superconducting solenoid of 6 m internal diameter providing an axial field of 3.8 T. Within the field volume are located the silicon pixel and strip tracker ($|\eta| < 2.4$) and the barrel and endcap calorimeters ($|\eta| < 3$); a lead tungstate crystal electromagnetic calorimeter and a brass/scintillator hadronic calorimeter. An iron/quartz-fiber calorimeter is located in the forward region ($3 < |\eta| < 5$), outside the field volume. For triggering purposes and to facilitate jet reconstruction, the calorimeter cells are grouped into towers projecting radially outward from the center of the detector.

3 Measurement of the invariant mass spectrum

3.1 Reconstruction and Trigger

The particle-flow (PF) algorithm [16, 17] is used to reconstruct the particles in an event and to identify them as muons, electrons, photons, and either charged or neutral hadrons.

Jets are reconstructed from either particles, giving PF-jets, or from calorimeter towers, giving Calo-jets. To reconstruct both types of jets we use the anti-k_t algorithm [31] with a distance parameter of 0.4, implemented in the FASTJET package [32]. For PF-jets, charged PF candidates not originating from the primary vertex are removed prior to the jet finding. For both types of jets, an event-by-event jet-area-based correction [33–35] is applied to the jets to remove the estimated energy from additional collisions in the same or adjacent bunch crossings (pileup).

Events are selected using a two-tier trigger system. Events satisfying loose jet requirements at the first level (L1) are examined by the high-level trigger (HLT). The high-level triggers use H_{T}, the scalar sum of the jet p_{T} from all jets in the event with $p_{\mathrm{T}} > 40\,\mathrm{GeV}$ and $|\eta| < 3$. For the high-mass search PF-jets are used to compute H_{T}, and events are accepted if they pass the HLT trigger requiring $H_{\mathrm{T}} > 800\,\mathrm{GeV}$. For the high-mass search we select events with $m_{\mathrm{jj}} > 1058\,\mathrm{GeV}$ for which the combined L1 trigger and HLT are found to be fully efficient. For the low-mass search, when an event passes the HLT trigger the jets reconstructed at the HLT are directly saved, along with a few other necessary objects reconstructed at HLT. The shorter time for event reconstruction and the reduced event size saved at HLT allows a reduced H_T threshold compared to the high-mass search. For the low-mass search Calo-jets are used to compute H_{T}, the threshold is $H_{\mathrm{T}} > 250\,\mathrm{GeV}$, and we select events with $m_{\mathrm{jj}} > 453\,\mathrm{GeV}$ for which the trigger is fully efficient.

3.2 Event pre-selection

At least one reconstructed vertex is required with $|z| < 24\,\mathrm{cm}$. The primary vertex is defined as the vertex with the highest sum of p_{T}^2 of the associated tracks. The jet momenta and energies are corrected using calibration constants obtained from simulation, test beam results, and pp collision data at $\sqrt{s} = 13\,\mathrm{TeV}$, using methods described in Ref. [35] with all *in situ* calibrations obtained from the current data. All jets are required to have $p_{\mathrm{T}} > 30\,\mathrm{GeV}$ and $|\eta| < 2.5$. The two jets with largest p_{T} are defined as the leading jets. Jet identification (ID) criteria are applied to remove spurious jets associated with calorimeter noise. The Jet ID for PF-jets is described in Ref. [36]. The Jet ID for Calo-jets requires that the fraction of jet energy deposited within the electromagnetic calorimeter be between 5% and 95% of the total jet energy. An event is rejected if either of the two leading jets does not satisfy the jet ID criteria.

3.3 Wide Jet Reconstruction and Event Selection

Geometrically close jets are combined into "wide jets" and used to determine the dijet mass, as in our previous searches [6–9]. The wide-jet algorithm, designed for dijet resonance event reconstruction, reduces the analysis sensitivity to gluon radiation from the final state partons. The two leading jets are used as seeds and the four-vectors of all other jets, if within $\Delta R = \sqrt{(\Delta\eta)^2 + (\Delta\phi)^2} < 1.1$, are added to the nearest leading jet to obtain two wide jets, which then form the dijet system. The background from t-channel dijet events is suppressed by requiring the pseudorapidity separation of the two wide jets to satisfy $|\Delta\eta_{\mathrm{jj}}| < 1.3$. The above requirements maximize the search sensitivity for isotropic decays of dijet resonances in the presence of QCD dijet background. For the low-mass search, after wide jet reconstruction and event selection, we use a correction derived from a smaller sample of *in situ* dijet data to calibrate the wide jets reconstructed from Calo-jet at HLT to have the same response as the wide jets reconstructed from PF-jets.

3.4 Dijet mass spectrum

Figure 1 shows the dijet mass spectra, defined as the observed number of events in each bin divided by the integrated luminosity and bin width, with predefined bins of width correspond-

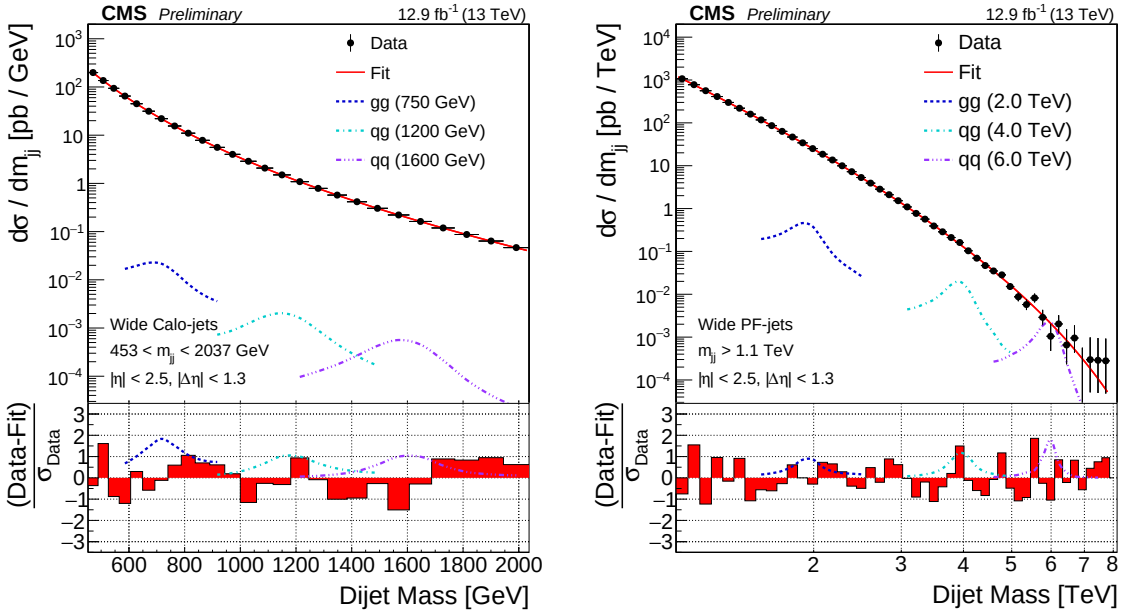

Figure 1: Dijet mass spectrum (points) compared to a fitted parameterization of the background (solid curve) for the low-mass search (left) and the high-mass search (right). The lower panel in each plot shows the difference between the data and the fitted parametrization, divided by the statistical uncertainty of the data. Predicted signals from narrow gluon-gluon, quark-gluon, and quark-quark resonances are shown with cross section equal to the observed upper limit at 95% CL.

ing to the dijet mass resolution [5]. The highest mass event has a dijet mass of 7.7 TeV and is shown in Fig. 2. The dijet mass spectra for the high-mass search and for the low-mass search

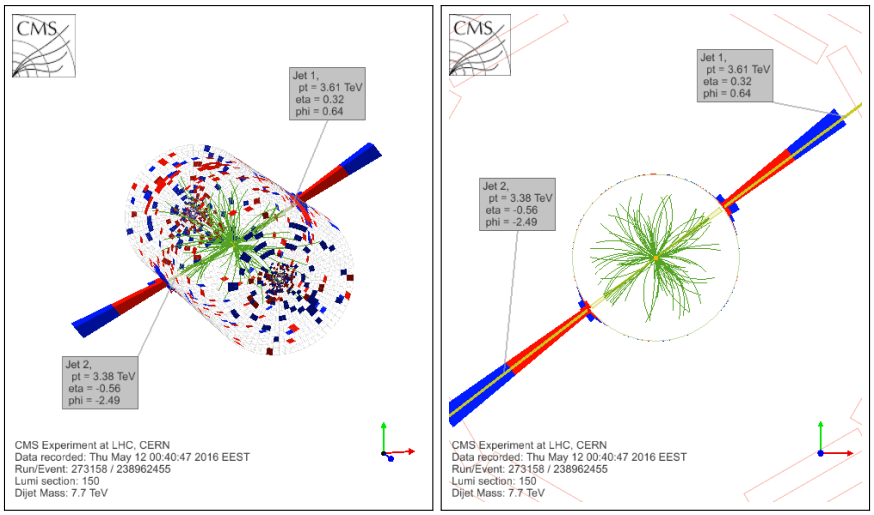

Figure 2: The event with the highest dijet invariant mass: three dimensional view (left), 2D view in the ρ-ϕ plane (right). The p_{T}, η, and ϕ values of the two wide jets are indicated. The invariant mass of the two wide jets is 7.7 TeV.

are fit with the following parameterization:

$$\frac{\mathrm{d}\sigma}{\mathrm{d}m_{\mathrm{jj}}} = \frac{P_0(1-x)^{P_1}}{x^{P_2+P_3\ln(x)}}\,, \tag{1}$$

where $x = m_{\mathrm{jj}}/\sqrt{s}$ and P_0, P_1, P_2, and P_3 are four fitted parameters. The functional form in Eq. 1 was also used in previous searches [1, 3–14, 37] to describe the data. In Fig. 1 we show the result of binned maximum likelihood fits, which yields the following chi-squared per number of degrees of freedom: $\chi^2/\mathrm{NDF} = 33.3/42$ for the high-mass search, $\chi^2/\mathrm{NDF} = 17.3/22$ for the low-mass search. The dijet mass spectra are well modeled by the background fits. In the lower panels of Fig. 1, in the region of dijet mass between 1.1 and 2 TeV, the bin-by-bin differences between the data and the background fit are not identical in the two searches because fluctuations in reconstructed dijet mass for calo-jets and pf-jets are not completely correlated.

4 Search

We search in the dijet mass spectrum for narrow resonances. Figure 3 shows examples of dijet mass distributions for simulated signal events generated with the PYTHIA 8 [38] program. The predicted mass distributions have Gaussian cores from the jet energy resolution, and tails towards lower mass values primarily from QCD radiation. The contribution of this low-mass tail to the lineshape depends on the parton content of the resonance (qq, qg, or gg). Resonances containing gluons, which emit QCD radiation more strongly than quarks, have a more pronounced tail. In Fig. 3, for a resonance mass of 750 GeV, we also show a hypothetical Gaussian shape with an RMS width of 10%, which is one of the widths used by the ATLAS experiment for their generic limits on Gaussian resonances. Fitting the core of the CMS qq resonance lineshape for calo-jets to a truncated Gaussian also gives an RMS width of approximately 10% at the resonance mass value of 750 GeV. Note that the expected distributions of dijet resonances

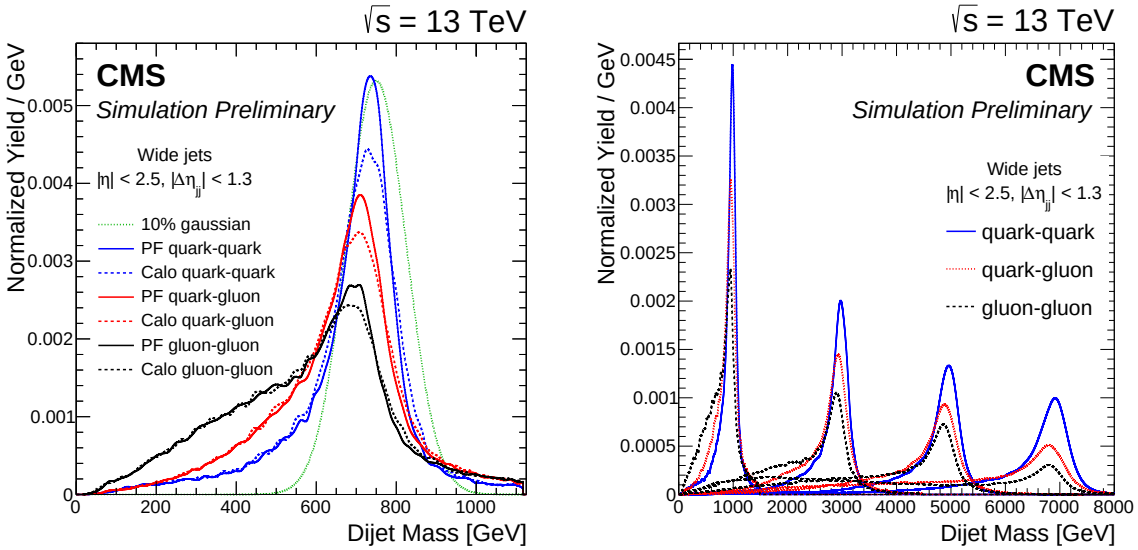

Figure 3: The reconstructed resonance mass spectrum predicted by the PYTHIA 8 MC event generator including simulation of the detector. Resonances from quark-quark processes modeled by $q\bar{q} \to G \to q\bar{q}$ (blue), quark-gluon processes modeled by $qg \to q^* \to qg$ (red), and gluon-gluon processes modeled by $gg \to G \to gg$ (black), where G is an RS graviton and q^* is an excited quark. (left) Resonances generated with a mass of 750 GeV are shown for wide jets from PF-jet reconstruction (solid) and calo-jet reconstruction (dashed). Also shown is a hypothetical Gaussian shape (dotted green) with a mean mass of 750 GeV and an RMS width equal to 10% of the mean mass. (right) Resonances generated with a mass of 1, 3, 5 and 7 TeV are shown for wide jets from PF-jet reconstruction.

from PYTHIA differ from a Gaussian shape centered at the resonance mass. This is primarily because of QCD radiation which produces significant tails and shifts the peak to a lower value of dijet mass. These real physical effects in the PYTHIA resonance shapes result in lower search sensitivity compared to hypothetical Gaussian shapes which neglect these effects.

Figure 1 includes our signal distributions of quark-quark, quark-gluon and gluon-gluon resonances with signal cross sections excluded at 95% CL by this analysis, as described below. There is no evidence for a narrow resonance in the data, as seen in Fig. 1. The most significant excess in the data relative to the background fit occurs in the low-mass search around 800 GeV in dijet mass. Fitting this data to a gluon-gluon resonance with a mass of 850 GeV yields a significance of 2.6 standard deviations.

5 Limits

We use the dijet mass spectrum from wide jets, the background parameterization, and the dijet resonance shapes to set limits on new particles decaying to the parton pairs qq (or $q\bar{q}$), qg, and gg. A separate limit is determined for each final state (qq, qg and gg) because of the dependence of the dijet resonance shape on the type of the two final-state partons.

The dominant sources of systematic uncertainty are the jet energy scale, jet energy resolution, integrated luminosity, and the estimation of background. The uncertainty in the jet energy scale is 2%, determined from Run 2 data using the methods described in Ref. [35]. This uncertainty is propagated to the limits by shifting the dijet mass shape for signal by $\pm 2\%$. The uncertainty in the jet energy resolution translates into an uncertainty of 10% in the resolution of the dijet mass [35], and is propagated to the limits by increasing and decreasing by 10% the reconstructed width of the dijet mass shape for signal. The uncertainty in the integrated luminosity is 6.2%, and is propagated to the normalization of the signal. Changes in the values of the parameters describing the background introduce a change in the signal strength that is accounted for as a systematic uncertainty.

The modified frequentist method [39, 40] is utilized to set upper limits on signal cross sections, following the prescription described in Ref. [41]. We use a multi-bin counting experiment likelihood, which is a product of Poisson distributions corresponding to different bins. We evaluate the likelihood independently at each value of resonance pole mass from 600 GeV to 1600 GeV in 50 GeV steps in the low-mass search, and from 1.6 TeV to 7.5 TeV in 100 GeV steps in the high-mass search. Gaussian distributions are used to model systematic uncertainties in the jet energy scale and jet energy resolution, and log normal distributions are used to model uncertainties in the integrated luminosity, treated as nuisance parameters within a constraint placed on the likelihood. For this methodology, the systematic uncertainty on the background is automatically evaluated via profiling, effectively refitting for the optimal values of the background parameters for each value of resonance cross section. The procedure gave the same limits as the Bayesian procedure used previously for dijet resonance searches at CMS [9]. For both the Bayesian and modified frequentist statistical procedures we find that the background systematic uncertainty has the largest effect on the limit. The amount the background uncertainty affects the limit depends significantly on the signal shape and the resonance mass, with the largest effect for the gluon-gluon resonances and the smallest effect for the hypothetical Gaussian resonances in the low-mass search, and the effect decreases as the resonance mass increases. The effect of systematics can be seen in the lower panels of Figure 1, where, for example, the excluded gg resonance signal at 750 GeV is more significantly above the data than is the excluded qq resonance signal at 6 TeV.

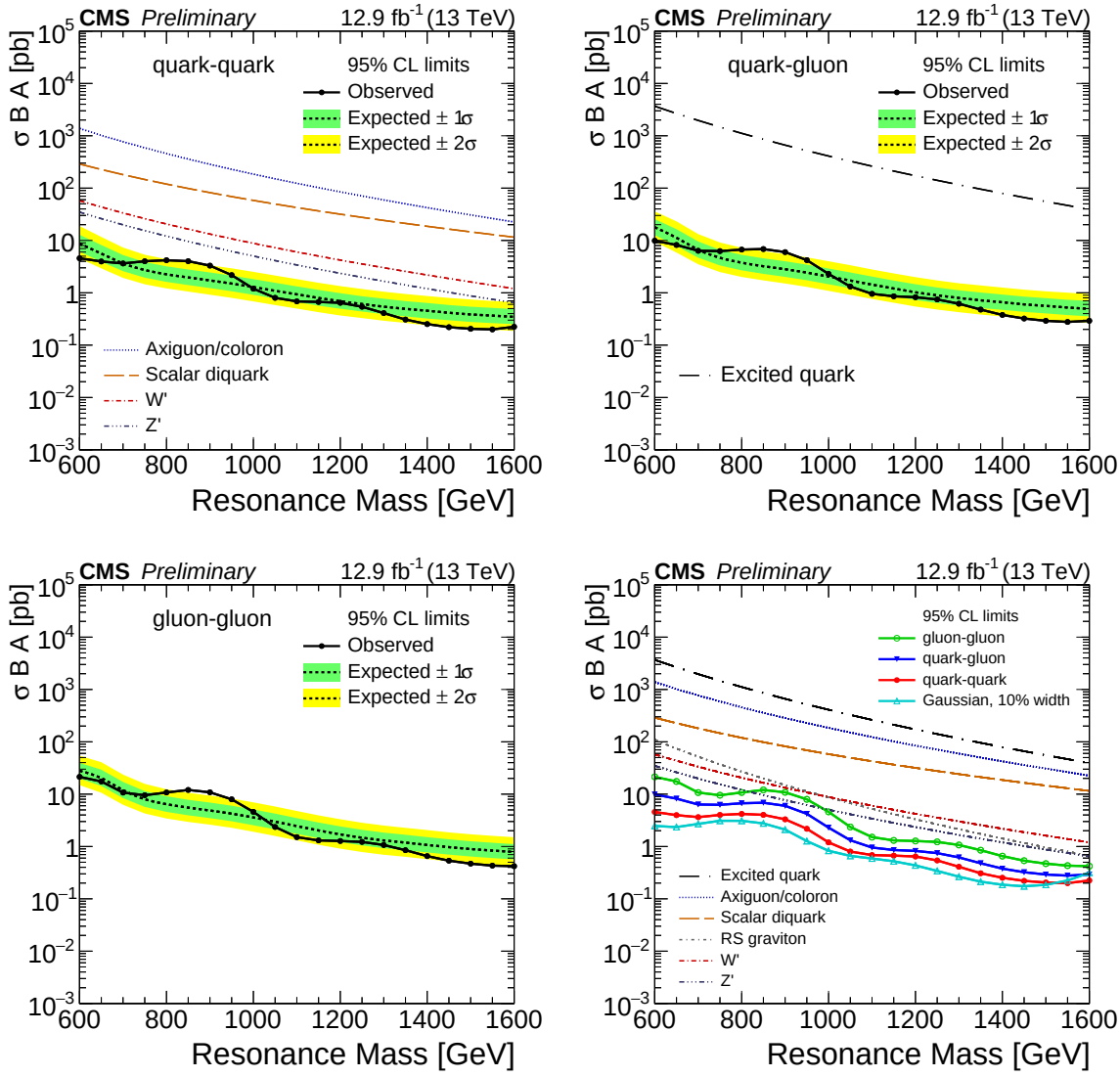

Figure 4: Limits from the low-mass search. The observed 95% CL upper limits on the product of the cross section, branching fraction, and acceptance for quark-quark (top left), quark-gluon (top right), and gluon-gluon (bottom left) type dijet resonances. The corresponding expected limits (dashed) and their variation at the 1 and 2 standard deviation levels (shaded bands) are also shown. (bottom right) The observed limits (solid) are summarized for fully simulated shapes from all three physical types of resonances along with the limit for a hypothetical Gaussian shape with RMS width equal to 10% of the mean mass. Limits are compared to the predicted cross sections of excited quarks [24, 25], axigluons [21], colorons [23], scalar diquarks [20], RS gravitons [28], and new gauge bosons W′ and Z′ [27].

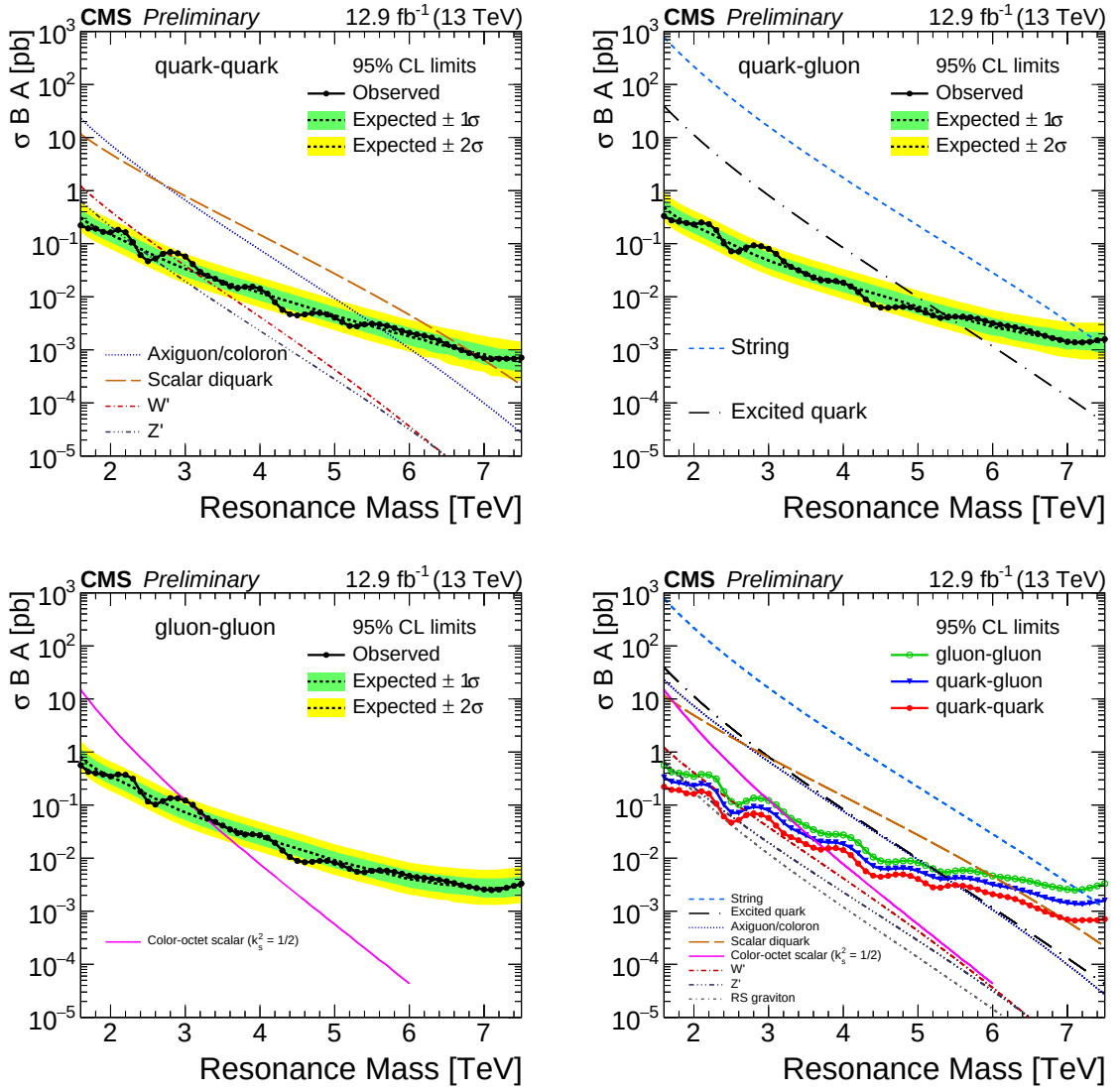

Figure 5: Limits from the high-mass search. The observed 95% CL upper limits on the product of the cross section, branching fraction, and acceptance for quark-quark (top left), quark-gluon (top right), and gluon-gluon (bottom left) type dijet resonances. The corresponding expected limits (dashed) and their variation at the 1 and 2 standard deviation levels (shaded bands) are also shown. (bottom right) The observed limits (solid) are summarized. Limits are compared to the predicted cross sections of string resonances [18, 19], excited quarks [24, 25], axigluons [21], colorons [23], scalar diquarks [20], color-octet scalars [26], new gauge bosons W′ and Z′ [27], and RS gravitons [28].

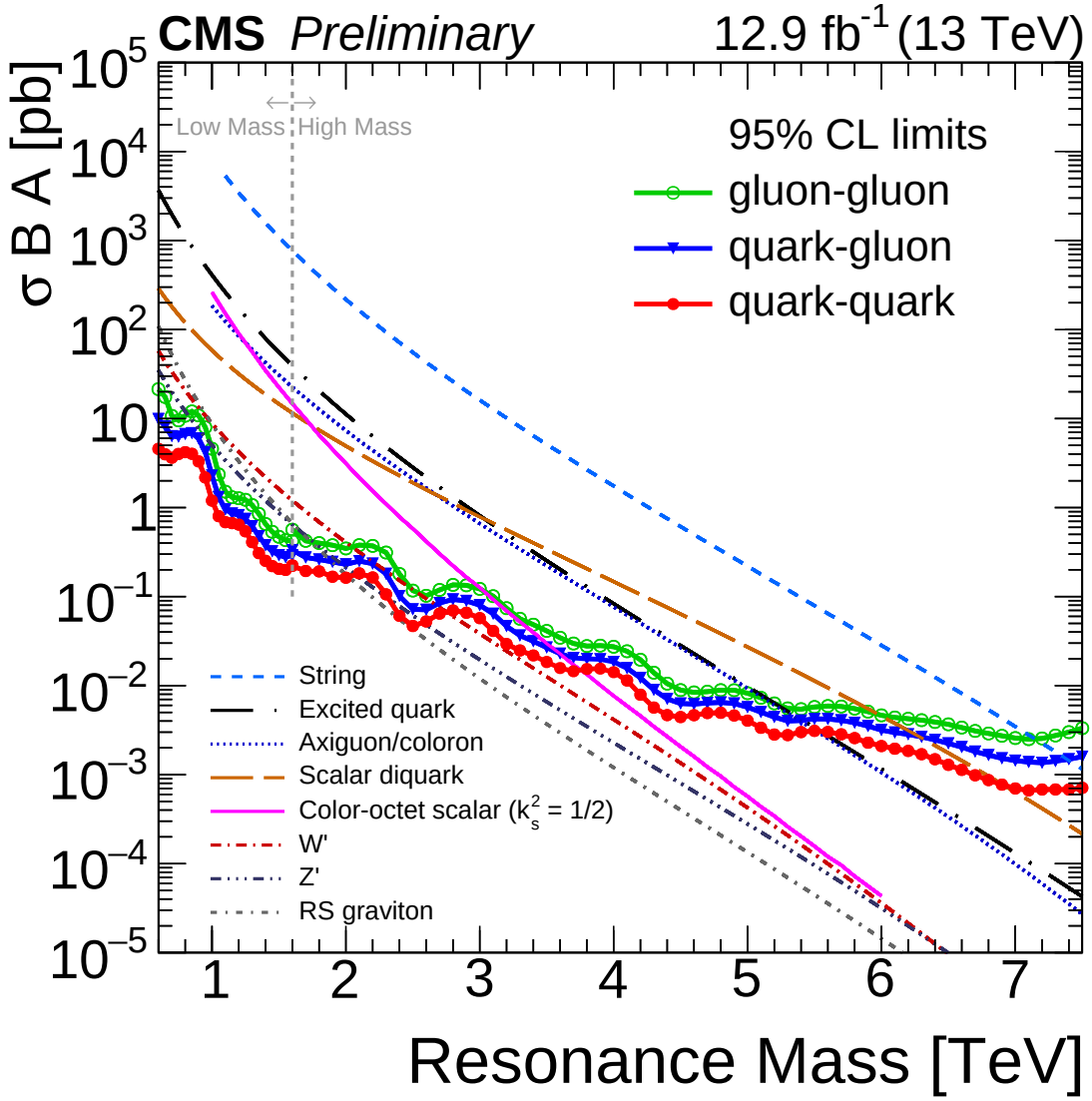

Figure 6: Limits from both the low-mass and high-mass search. The observed 95% CL upper limits on the product of the cross section, branching fraction, and acceptance for quark-quark, quark-gluon, and gluon-gluon type dijet resonances. The observed limits (solid) are presented from the low mass search, for resonance masses between 0.6 TeV and 1.6 TeV, and from the high mass search for resonance masses greater than or equal to 1.6 TeV. Limits are compared to the predicted cross sections of string resonances [18, 19], excited quarks [24, 25], axigluons [21], colorons [23], scalar diquarks [20], color-octet scalars [26], new gauge bosons W′ and Z′ [27], and RS gravitons [28].

Figures 4-6 show the model-independent observed upper limits at 95% confidence level (CL) on $\sigma\, B\, A$, i.e., the product of the cross section (σ), the branching fraction (B), and the acceptance (A) for the kinematic requirements $|\Delta\eta_{jj}| < 1.3$ and $|\eta| < 2.5$, for narrow resonances. In Fig 4, for comparison purposes only, limits are also shown from Gaussian shapes with an RMS width equal to 10% of the mass. The acceptance of the minimum dijet mass requirement in each search has been taken into account by correcting the limits, and therefore does not appear in the acceptance A. Figures 4-6 also show the expected limits on the cross section and their bands of uncertainty. The generated mass spectra are fit with a signal+background model to extract expected upper limits. The difference in the limits for qq, qg, gg and Gaussian resonances at the same resonance mass originates from the difference in their lineshapes. We note that the limits from Gaussian resonances are smaller than can be expected from any physical model, as they do not have any tails due to radiation, and consequently they are narrower and located closer to the resonance pole than any combination of two partons can produce.

All upper limits presented can be compared to the parton-level predictions of $\sigma\, B\, A$, without detector simulation, to determine mass limits on new particles. The model predictions shown in Fig. 4-6 are calculated in the narrow-width approximation [15] using the CTEQ6L1 [42] PDF at leading order, with a next-to-leading order correction factor included for the W′, Z′, and axigluon/coloron models [22]. The acceptance is evaluated at the parton level for the resonance decay to two partons. In the case of isotropic decays it is $A \approx 0.6$ independent of resonance mass. For a given model, new particles are excluded at 95% CL in mass regions where the theoretical prediction lies at or above the observed upper limit for the appropriate final state of Fig. 4-6. For the RS graviton model, for which 60%(40%) of the cross section comes from sub-proceses with only quarks(gluons) in the final state, we obtain mass limits by comparing the RS graviton cross section curve to a weighted average of the limits in the quark-quark and gluon-gluon final states. The mass limits are reported in Table 1 for all models.

Table 1: Observed and expected mass limits at 95% CL from this analysis with 12.9 fb^{-1} at $\sqrt{s} = 13$ TeV compared to previously published limits on narrow resonances from CMS with 2.4 fb^{-1} at $\sqrt{s} = 13$ TeV [3] and with 20 fb^{-1} at $\sqrt{s} = 8$ TeV [9]. The listed models are excluded between 0.6 TeV and the indicated mass limit by this analysis. For the Z′ model, in addition to the observed mass limit listed below, this analysis also excludes the mass interval between 2.3 and 2.6 TeV.

		Observed (expected) mass limit [TeV]		
Model	Final State	12.9 fb^{-1} 13 TeV	2.4 fb^{-1} 13 TeV	20 fb^{-1} 8 TeV
String	qg	7.4 (7.4)	7.0 (6.9)	5.0 (4.9)
Scalar diquark	qq	6.9 (6.8)	6.0 (6.1)	4.7 (4.4)
Axigluon/coloron	$q\bar{q}$	5.5 (5.6)	5.1 (5.1)	3.7 (3.9)
Excited quark	qg	5.4 (5.4)	5.0 (4.8)	3.5 (3.7)
Color-octet scalar ($k_s^2 = 1/2$)	gg	3.0 (3.3)	—	—
W′	$q\bar{q}$	2.7 (3.1)	2.6 (2.3)	2.2 (2.2)
Z′	$q\bar{q}$	2.1 (2.3)	—	1.7 (1.8)
RS Graviton	$q\bar{q}$, gg	1.9 (1.8)	—	1.6 (1.3)

We have presented limits with Gaussian shapes of 10% width in order to compare the sensitivity of this search to the tails of the signal shape, and the sensitivity of these results with those from ATLAS in Ref. [2] which presents results using the same Gaussian shape. Our limit on $\sigma\, B\, A$ with the Gaussian shape of 10% width at 750 GeV is 1.8 pb expected, and the previous ATLAS limit in Ref. [2] was 2.4 pb for a luminosity of 3.4 fb^{-1}. We note that the ATLAS analysis

used $|\Delta\eta_{jj}| < 1.2$ which gives 93% of the acceptance of CMS for an isotropic signal. After adjusting for differences in luminosity and acceptance between the two analyses the CMS and ATLAS sensitivities to a Gaussian resonance of mass 750 GeV and width 10% are similar. We also note that at this resonance mass for this signal shape our reported limit, which includes systematic uncertainties, is 60% larger than the limit obtained without including systematic uncertainties. For a gluon-gluon resonance at a mass of 750 GeV, systematic uncertainties increase the limit by a factor of 3, a significantly larger effect than for a Gaussian resonance which neglects the effect of radiation. Our limits on hypothetical Gaussian resonances are only recommended for such comparisons, as we have demonstrated that these Gaussian shapes neglect the sizable tails due to QCD radiation, and are consequently more narrow and result in significantly better limits than can be physically expected for any pair of partons.

6 Conclusions

In summary, two searches for narrow resonances decaying into a pair of jets have been performed using pp collisions at $\sqrt{s} = 13$ TeV corresponding to an integrated luminosity of 12.9 fb^{-1}. A low-mass search using data scouting from the HLT trigger with calorimeter jets and a high-mass search using particle flow jets. The dijet mass spectra have been measured to be smoothly falling distributions. In the analyzed data samples, there is no evidence for resonant particle production. We present generic upper limits on the product $\sigma\, B\, A$ for narrow quark-quark, quark-gluon and gluon-gluon resonances that are applicable to any model of narrow dijet resonance production. We set mass limits at 95% CL on models of string resonances, scalar diquarks, excited quarks, axigluons, colorons, color octet scalars, W′ bosons, Z′ bosons, and RS gravitons, which extend previously published limits in the dijet channel.

References

[1] CMS Collaboration, "Search for narrow resonances in dijet final states at $\sqrt{(s)} = 8$ TeV with the novel CMS technique of data scouting", *Phys. Rev. Lett.* **117** (2016), no. 3, 031802, doi:10.1103/PhysRevLett.117.031802, arXiv:1604.08907.

[2] ATLAS Collaboration, "Search for light dijet resonances with the ATLAS detector using a Trigger-Level Analysis in LHC pp collisions at $\sqrt{s} = 13$ TeV", ATLAS Conference Report ATLAS-CONF-2016-030, Jun, 2016.

[3] CMS Collaboration, "Search for narrow resonances decaying to dijets in proton-proton collisions at $\sqrt{s} = 13$ TeV", *Phys. Rev. Lett.* **116** (2016) 071801, doi:10.1103/PhysRevLett.116.071801, arXiv:1512.01224.

[4] ATLAS Collaboration, "Search for new phenomena in dijet mass and angular distributions from pp collisions at $\sqrt{s} = 13$ TeV with the ATLAS detector", *Phys. Lett.* **B754** (2016) 302–322, doi:10.1016/j.physletb.2016.01.032, arXiv:1512.01530.

[5] CMS Collaboration, "Search for Dijet Resonances in 7 TeV pp Collisions at CMS", *Phys. Rev. Lett.* **105** (2010) 211801, doi:10.1103/PhysRevLett.105.211801, arXiv:1010.0203. [Erratum doi:10.1103/PhysRevLett.106.029902].

[6] CMS Collaboration, "Search for resonances in the dijet mass spectrum from 7 TeV pp collisions at CMS", *Phys. Lett. B* **704** (2011) 123, doi:10.1016/j.physletb.2011.09.015, arXiv:1107.4771.

[7] CMS Collaboration, "Search for narrow resonances and quantum black holes in inclusive and b-tagged dijet mass spectra from pp collisions at $\sqrt{s} = 7$ TeV", *JHEP* **01** (2013) 013, doi:10.1007/JHEP01(2013)013, arXiv:1210.2387.

[8] CMS Collaboration, "Search for narrow resonances using the dijet mass spectrum in pp collisions at $\sqrt{s} = 8$ TeV", *Phys. Rev. D* **87** (2013) 114015, doi:10.1103/PhysRevD.87.114015, arXiv:1302.4794.

[9] CMS Collaboration, "Search for resonances and quantum black holes using dijet mass spectra in proton-proton collisions at $\sqrt{s} = 8$ TeV", *Phys. Rev. D* **91** (2015) 052009, doi:10.1103/PhysRevD.91.052009, arXiv:1501.04198.

[10] ATLAS Collaboration, "Search for New Particles in Two-Jet Final States in 7 TeV Proton-Proton Collisions with the ATLAS Detector at the LHC", *Phys. Rev. Lett.* **105** (2010) 161801, doi:10.1103/PhysRevLett.105.161801, arXiv:1008.2461.

[11] ATLAS Collaboration, "Search for new physics in dijet mass and angular distributions in pp collisions at $\sqrt{s} = 7$ TeV measured with the ATLAS detector", *New J. Phys.* **13** (2011) 053044, doi:10.1088/1367-2630/13/5/053044, arXiv:1103.3864.

[12] ATLAS Collaboration, "Search for new physics in the dijet mass distribution using 1 fb^{-1} of pp collision data at $\sqrt{s} = 7$ TeV collected by the ATLAS detector", *Phys. Lett. B* **708** (2012) 37, doi:10.1016/j.physletb.2012.01.035, arXiv:1108.6311.

[13] ATLAS Collaboration, "ATLAS search for new phenomena in dijet mass and angular distributions using pp collisions at $\sqrt{s} = 7$ TeV", *JHEP* **01** (2013) 029, doi:10.1007/JHEP01(2013)029, arXiv:1210.1718.

[14] ATLAS Collaboration, "Search for new phenomena in the dijet mass distribution using pp collision data at $\sqrt{s} = 8$ TeV with the ATLAS detector", *Phys. Rev. D* **91** (2015) 052007, doi:10.1103/PhysRevD.91.052007, arXiv:1407.1376.

[15] R. M. Harris and K. Kousouris, "Searches for dijet resonances at hadron colliders", *Int. J. Mod. Phys. A* **26** (2011) 5005, doi:10.1142/S0217751X11054905, arXiv:1110.5302.

[16] CMS Collaboration, "Particle–Flow Event Reconstruction in CMS and Performance for Jets, Taus, and $E_{\mathrm{T}}^{\mathrm{miss}}$", CMS Physics Analysis Summary CMS-PAS-PFT-09-001, 2009.

[17] CMS Collaboration, "Commissioning of the Particle-flow Event Reconstruction with the first LHC collisions recorded in the CMS detector", CMS Physics Analysis Summary CMS-PAS-PFT-10-001, 2010.

[18] L. A. Anchordoqui et al., "Dijet Signals for Low Mass Strings at the LHC", *Phys. Rev. Lett.* **101** (2008) 241803, doi:10.1103/PhysRevLett.101.241803, arXiv:0808.0497.

[19] S. Cullen, M. Perelstein, and M. E. Peskin, "TeV strings and collider probes of large extra dimensions", *Phys. Rev. D* **62** (2000) 055012, doi:10.1103/PhysRevD.62.055012, arXiv:hep-ph/0001166.

[20] J. L. Hewett and T. G. Rizzo, "Low-energy phenomenology of superstring-inspired E(6) models", *Phys. Rept.* **183** (1989) 193, doi:10.1016/0370-1573(89)90071-9.

[21] P. H. Frampton and S. L. Glashow, "Chiral Color: An Alternative to the Standard Model", *Phys. Lett. B* **190** (1987) 157, doi:10.1016/0370-2693(87)90859-8.

[22] R. S. Chivukula, E. H. Simmons, A. Farzinnia, and J. Ren, "Hadron collider production of massive color-octet vector bosons at next-to-leading order", *Phys. Rev. D* **87** (2013) 094011, doi:10.1103/PhysRevD.87.094011, arXiv:1303.1120.

[23] E. H. Simmons, "Coloron phenomenology", *Phys. Rev. D* **55** (1997) 1678, doi:10.1103/PhysRevD.55.1678, arXiv:hep-ph/9608269.

[24] U. Baur, I. Hinchliffe, and D. Zeppenfeld, "Excited Quark Production at Hadron Colliders", *Int. J. Mod. Phys. A* **02** (1987) 1285, doi:10.1142/S0217751X87000661.

[25] U. Baur, M. Spira, and P. M. Zerwas, "Excited quark and lepton production at hadron colliders", *Phys. Rev. D* **42** (1990) 815, doi:10.1103/PhysRevD.42.815.

[26] T. Han, I. Lewis, and Z. Liu, "Colored resonant signals at the LHC: largest rate and simplest topology", *JHEP* **12** (2010) 085, doi:10.1007/JHEP12(2010)085, arXiv:1010.4309.

[27] E. Eichten, I. Hinchliffe, K. D. Lane, and C. Quigg, "Supercollider physics", *Rev. Mod. Phys.* **56** (1984) 579, doi:10.1103/RevModPhys.56.579.

[28] L. Randall and R. Sundrum, "An Alternative to compactification", *Phys. Rev. Lett.* **83** (1999) 4690, doi:10.1103/PhysRevLett.83.4690, arXiv:hep-th/9906064.

[29] R. Sekhar Chivukula, E. H. Simmons, and N. Vignaroli, "Distinguishing dijet resonances at the LHC", *Phys. Rev.* **D91** (2015), no. 5, 055019, doi:10.1103/PhysRevD.91.055019, arXiv:1412.3094.

[30] CMS Collaboration, "The CMS experiment at the CERN LHC", *JINST* **3** (2008) S08004, doi:10.1088/1748-0221/3/08/S08004.

[31] M. Cacciari, G. P. Salam, and G. Soyez, "The Anti-k_t jet clustering algorithm", *JHEP* **04** (2008) 063, doi:10.1088/1126-6708/2008/04/063, arXiv:0802.1189.

[32] M. Cacciari and G. P. Salam, "Dispelling the N^3 myth for the k_t jet-finder", *Phys. Lett. B* **641** (2006) 57, doi:10.1016/j.physletb.2006.08.037, arXiv:hep-ph/0512210.

[33] M. Cacciari, G. P. Salam, and G. Soyez, "FastJet user manual", *Eur. Phys. J. C* **72** (2012) 1896, doi:10.1140/epjc/s10052-012-1896-2, arXiv:1111.6097.

[34] M. Cacciari and G. P. Salam, "Pileup subtraction using jet areas", *Phys. Lett. B* **659** (2008) 119, doi:10.1016/j.physletb.2007.09.077, arXiv:0707.1378.

[35] CMS Collaboration, "Jet energy scale and resolution in the CMS experiment in pp collisions at 8 TeV", (2016). arXiv:1607.03663. Submitted to JINST.

[36] CMS Collaboration, "Jet Performance in pp Collisions at $\sqrt{s} = 7$ TeV", CMS Physics Analysis Summary CMS-PAS-JME-10-003, 2010.

[37] CDF Collaboration, "Search for new particles decaying into dijets in proton-antiproton collisions at $\sqrt{s} = 1.96$ TeV", *Phys. Rev. D* **79** (2009) 112002, doi:10.1103/PhysRevD.79.112002, arXiv:0812.4036.

[38] T. Sjöstrand, S. Mrenna, and P. Skands, "A brief introduction to PYTHIA 8.1", *Comp. Phys. Comm.* **178** (2008) 852, doi:10.1016/j.cpc.2008.01.036, arXiv:0710.3820.

[39] T. Junk, "Confidence level computation for combining searches with small statistics", *Nucl. Instr. and Meth. A* **434** (1999) 435, doi:10.1016/S0168-9002(99)00498-2, arXiv:hep-ex/9902006.

[40] A. L. Read, "Presentation of search results: the CL_s technique", *J. Phys. G* **28** (2002) 2693, doi:10.1088/0954-3899/28/10/313.

[41] LHC Higgs Combination Group, "Procedure for the LHC Higgs boson search combination in Summer 2011", Technical Report CMS-NOTE-2011-005, ATL-PHYS-PUB-2011-11, 2011.

[42] J. Pumplin et al., "New generation of parton distributions with uncertainties from global QCD analysis", *JHEP* **07** (2002) 012, doi:10.1088/1126-6708/2002/07/012, arXiv:hep-ph/0201195.